





## An organic/inorganic hybrid soft material for supramolecular adhesion†

 Yunfei Zhang, Wenchang Yi, Jia Pan, Song Liu \* and Shengyi Dong \*

 Cite this: *Soft Matter*, 2024, 20, 5670

 Received 27th April 2024,  
 Accepted 24th June 2024

DOI: 10.1039/d4sm00501e

[rsc.li/soft-matter-journal](https://rsc.li/soft-matter-journal)

Thioctic acid (TA) has been widely used to construct soft materials via supramolecular copolymerization with organic chemicals. In this study, TA and the inorganic compound MoS<sub>2</sub> are used to fabricate poly[TA-MoS<sub>2</sub>] via dynamic covalent and supramolecular interactions. Poly[TA-MoS<sub>2</sub>] exhibits good and long-lasting adhesion performance on various artificial surfaces, with an adhesion strength up to 3.72 MPa (15 days). Further, it exhibits tough adhesion effects in an aqueous environment. Moreover, poly[TA-MoS<sub>2</sub>] displays good thermal processing behavior, thus enabling its molding through 3D printing.

Thioctic acid (TA) is a natural coenzyme and plays a significant role in our life activities.<sup>1–6</sup> Recently, TA and its structure-modified derivatives have been widely applied as main building blocks in supramolecular assembly and dynamic polymerization, according to the pioneering work of Qu *et al.*<sup>7–10</sup> Various materials with attractive properties, functions, and applications have been designed and constructed through thermally induced ring-opening polymerization of TA with different additives.<sup>11–14</sup>

Poly[TA] is a hard and fragile thermoplastic material that can be easily modified using various additives through covalent and/or supramolecular cross-linking.<sup>15–19</sup> The incorporation of functional chemicals endows poly[TA] with multiple amazing properties, such as self-healing, conductivity, elasticity, and adhesion properties.<sup>20–24</sup> To date, the majority of additives used in poly[TA] systems are restricted to organic compounds, including ionic liquids, fluorescent molecules, and natural acids/sugars.<sup>25–29</sup> In contrast, inorganic molecules have been less used in the fabrication of functional poly[TA] materials because of the lack of compatibility between TA and inorganic components.<sup>30</sup> Considering that more choices of additives can give rise to more flexibility in the properties and functions of

poly[TA] materials, it is of great importance to study the combination of poly[TA] with inorganic additives.

Herein, an organic/inorganic hybrid supramolecular adhesive was constructed through solvent-free non-covalent polymerization of TA and MoS<sub>2</sub>. The molecular recognition between TA and MoS<sub>2</sub> not only yielded strong supramolecular adhesion, but also greatly improved the thermal processability of poly[TA].

Poly[TA-MoS<sub>2</sub>] was easily synthesized by directly stirring the powder mixture of TA and MoS<sub>2</sub> at 130 °C for 120 minutes (Fig. 1a). This facile preparation method allows for the preparation of poly[TA-MoS<sub>2</sub>] on a large scale (>1 kg). For poly[TA-MoS<sub>2</sub>], the infrared (IR) peak of the C=O groups shifted from 1686 to 1699 cm<sup>-1</sup>, suggesting the supramolecular interaction between TA and MoS<sub>2</sub> (Fig. 1b). X-ray photoelectron spectroscopy-based characterization of poly[TA-MoS<sub>2</sub>] showed that the Mo 3d<sub>5/2</sub> orbital peak was shifted from 228.36 eV to 227.04 eV, indicating metal coordination between poly[TA] and MoS<sub>2</sub> (Fig. 1c and Fig. S1, ESI†).<sup>31</sup> Meanwhile, scanning electron microscopy and atomic force microscopy data show that poly[TA-MoS<sub>2</sub>] contained dense and nonporous microscopic structures, in which poly[TA] and MoS<sub>2</sub> molecules were uniformly distributed (Fig. S2–S4, ESI†).

The obtained poly[TA-MoS<sub>2</sub>] was stable at high temperatures or in the presence of water. According to the thermogravimetric analysis experiments of poly[TA-MoS<sub>2</sub>], its thermal degradation temperature was higher than 225 °C (Fig. S5, ESI†). Meanwhile, after storing poly[TA-MoS<sub>2</sub>] underwater for 35 days, it was intact, and no dissolution phenomenon of TA or poly[TA] was recorded (Fig. S6 and S7, ESI†). In addition, the time-dependent IR spectra of poly[TA-MoS<sub>2</sub>] intuitively demonstrate its long-term stability because neither new peaks nor obvious shifts were observed when the IR spectra of freshly prepared poly[TA-MoS<sub>2</sub>] samples were compared with those of the long-term stored samples (Fig. S8, ESI†).

Before studying the adhesion capacity, the glass-transition temperature (*T*<sub>g</sub>) and rheological performance of poly[TA-MoS<sub>2</sub>] were measured because the *T*<sub>g</sub> value and rheological behavior are closely related to the adhesion capacity of a material. Low *T*<sub>g</sub>

College of Chemistry and Chemical Engineering, Hunan University, Changsha 410082, China. E-mail: [dongsy@hnu.edu.cn](mailto:dongsy@hnu.edu.cn), [liusong@hnu.edu.cn](mailto:liusong@hnu.edu.cn)

† Electronic supplementary information (ESI) available. See DOI: <https://doi.org/10.1039/d4sm00501e>

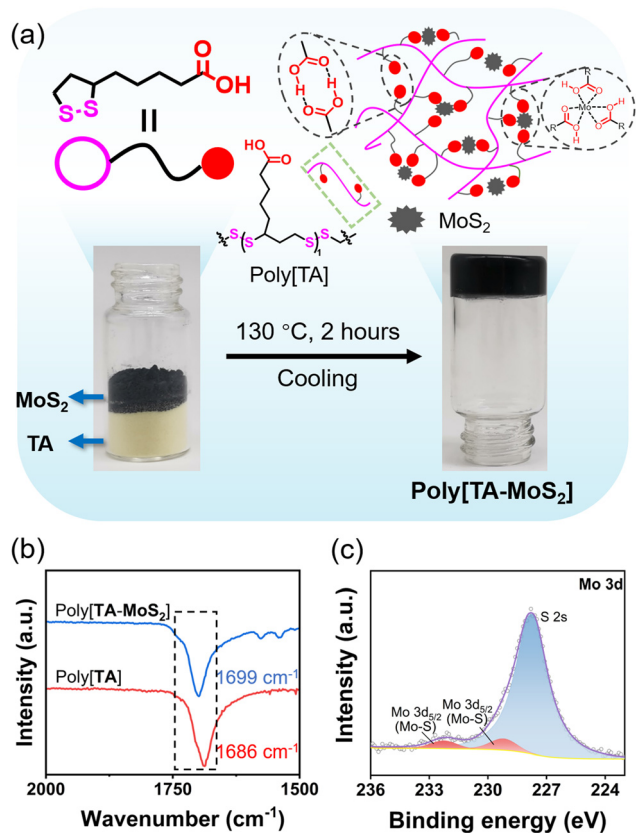


Fig. 1 The preparation and characterization of poly[TA-MoS<sub>2</sub>]. (a) The formation of poly[TA-MoS<sub>2</sub>]; (b) partial FT-IR spectra of poly[TA] and poly[TA-MoS<sub>2</sub>]; (c) XPS spectrum of Mo 3d in [TA-MoS<sub>2</sub>] (TA : MoS<sub>2</sub> = 10 : 1).

and  $T_m$  values of  $-9.7$  °C and  $90.48$  °C were obtained from the differential scanning calorimetric spectra of poly[TA-MoS<sub>2</sub>], respectively, indicating that poly[TA-MoS<sub>2</sub>] is a suitable hot-molten adhesive rather than a pressure-sensitive adhesive (Fig. S9, ESI<sup>†</sup>). The dynamic thermomechanical and rheological analysis results clearly showed high values of storage modulus and viscosity for poly[TA-MoS<sub>2</sub>] under room temperature, indicating its excellent elasticity and stretchability (Fig. S10–S14, ESI<sup>†</sup>). Meanwhile, when the temperature was  $>60$  °C, the value of storage modulus was lower than the loss modulus, manifesting that at high temperatures, poly[TA-MoS<sub>2</sub>] exists as a liquid rather than a solid, and the transition from a solid to a viscous liquid was observed by the naked eye when a piece of poly[TA-MoS<sub>2</sub>] sample was heated.

Poly[TA-MoS<sub>2</sub>] showed strong adhesion effects on artificial substrates (Fig. 2). The adhesion strengths of poly[TA-MoS<sub>2</sub>]<sub>1/1</sub>, which was taken as the typical example, to glass and polymethyl methacrylate (PMMA) were 1.50 and 1.47 MPa (2 h), which are close to those of organic chemical-doped TA materials.<sup>32–35</sup> Meanwhile, it is known that an appropriate ratio of poly[TA]/MoS<sub>2</sub> is essential to realizing tough adhesion performance. Poly[TA-MoS<sub>2</sub>] with higher MoS<sub>2</sub> content showed better adhesion capacity. Poly[TA-MoS<sub>2</sub>]<sub>1/1</sub>, poly[TA-MoS<sub>2</sub>]<sub>5/1</sub>, poly[TA-MoS<sub>2</sub>]<sub>10/1</sub>, and poly[TA-MoS<sub>2</sub>]<sub>100/1</sub> showed high adhesion strengths on steel, measuring 2.10, 1.73, 1.30, and 1.04 MPa (2 h), respectively, clearly

demonstrating the importance of MoS<sub>2</sub> in supramolecular adhesion. On extending the adhesion time, the adhesion strength of poly[TA-MoS<sub>2</sub>] remained stable. The measured adhesion strengths of poly[TA-MoS<sub>2</sub>]<sub>100/1</sub> to glass were 0.80 (2 h), 0.75 (1 day), 0.80 (3 days), and 0.78 MPa (15 days). Similar adhesion performance was observed for poly[TA-MoS<sub>2</sub>] with other ratios. A brief comparison of the adhesion strengths of poly[TA-MoS<sub>2</sub>] and other reported TA-based adhesives is presented in Fig. S15 (ESI<sup>†</sup>). Macroscopic tests directly confirmed the good adhesion effect of poly[TA-MoS<sub>2</sub>]. No adhesion failure was found when two plates adhered by poly[TA-MoS<sub>2</sub>] were hung with a weight of 4 kg (Fig. 2e). In addition, as the temperature increased, the adhesion strength of poly[TA-MoS<sub>2</sub>] decreased. Therefore, poly[TA-MoS<sub>2</sub>] is not suitable for adhesion at high temperatures (Fig. S16 and S17, ESI<sup>†</sup>).

Poly[TA-MoS<sub>2</sub>] did not only display good adhesion at ambient conditions but also under water. When poly[TA-MoS<sub>2</sub>] was immersed under water for 2 h, no obvious decay in the adhesion strength was observed (Fig. 2e). For example, the underwater adhesion strength of poly[TA-MoS<sub>2</sub>]<sub>1/1</sub> on glass was 1.52 MPa (2 h), which is close to that obtained without water. However, poly[TA-MoS<sub>2</sub>]<sub>100/1</sub> displayed relatively poor adhesion capacity when the adhesion tests were performed in the presence of water. The underwater adhesion strengths of poly[TA-MoS<sub>2</sub>]<sub>100/1</sub> to glass and PMMA were only 68.75% and 62.67% of those obtained without water, respectively (Fig. 3). The good underwater adhesion of poly[TA-MoS<sub>2</sub>] is attributed to the following aspects: (i) poly[TA-MoS<sub>2</sub>] can thoroughly cover the adhesion area of the substrates, and thus, water molecules cannot attenuate the adhesion effects by forming hydrogen bonding with the hydrophilic groups on the surfaces of the tested substrates; (ii) poly[TA-MoS<sub>2</sub>] is water insoluble, meaning that the adhesion layer cannot be destroyed by water. Additionally, it was found that extending the underwater adhesion time obviously yielded a stronger adhesion effect. For example, when the adhesion time was 3 and 15 days, the adhesion strengths of poly[TA-MoS<sub>2</sub>]<sub>1/1</sub> on steel were 3.19 and 3.26 MPa, respectively. Similar enhanced adhesion effects were observed, when poly[TA-MoS<sub>2</sub>]<sub>10/1</sub> and poly[TA-MoS<sub>2</sub>-TA-MoS<sub>2</sub>]<sub>100/1</sub> were used in the adhesion tests.

It has been reported that poly[TA] and its derivatives can be obtained by light irradiation at 420 nm without heating.<sup>36–38</sup> In the following adhesion study, the on-site adhesion potential of poly[TA-MoS<sub>2</sub>] was carefully investigated. A mixture of TA and MoS<sub>2</sub> powders was sandwiched by two glass plates and irradiated at 420 nm. Macroscopic tests showed that two plates were firmly adhered together after irradiation. Meanwhile, no obvious heating effect was observed during the on-site preparation and adhesion processes. Poly[TA-MoS<sub>2</sub>] prepared by this irradiation method displayed good adhesion performance on glass. The adhesion strengths of poly[TA-MoS<sub>2</sub>]<sub>1/1</sub>, poly[TA-MoS<sub>2</sub>]<sub>5/1</sub>, poly[TA-MoS<sub>2</sub>]<sub>10/1</sub>, and poly[TA-MoS<sub>2</sub>]<sub>100/1</sub> to glass were 0.93, 0.87, 0.68, and 0.43 MPa, respectively, when they were irradiated for only 2 min (Fig. 4b).

Inspired by the results of the light-induced supramolecular adhesion of poly[TA-MoS<sub>2</sub>], more light conditions were tested.<sup>39,40</sup>

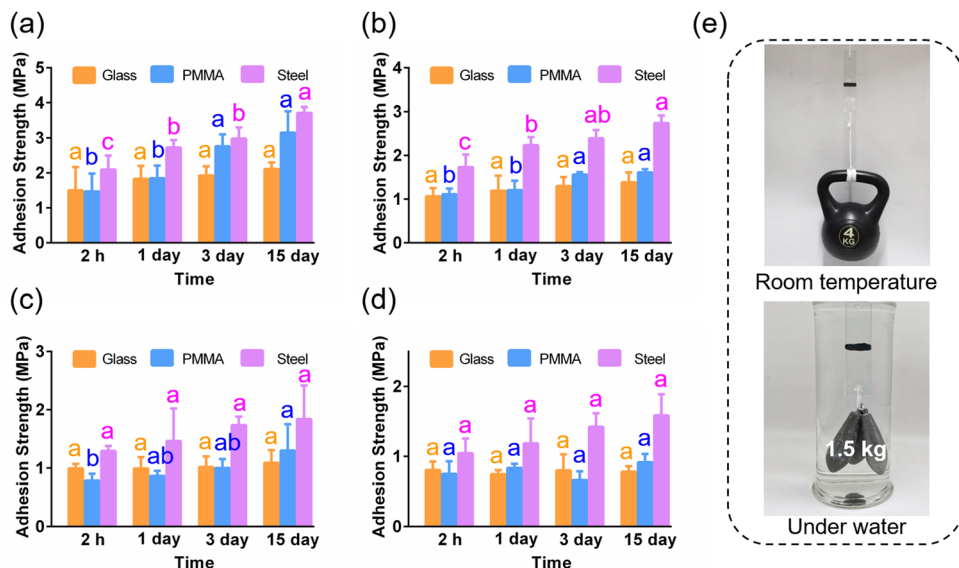


Fig. 2 Time-dependent adhesion strengths of poly[TA-MoS<sub>2</sub>]. (a) TA : MoS<sub>2</sub> = 1 : 1; (b) TA : MoS<sub>2</sub> = 5 : 1; (c) TA : MoS<sub>2</sub> = 10 : 1; (d) TA : MoS<sub>2</sub> = 100 : 1; (e) macroscopic adhesion behavior of poly[TA-MoS<sub>2</sub>]. Different letters signify significant differences at  $p < 0.05$ .

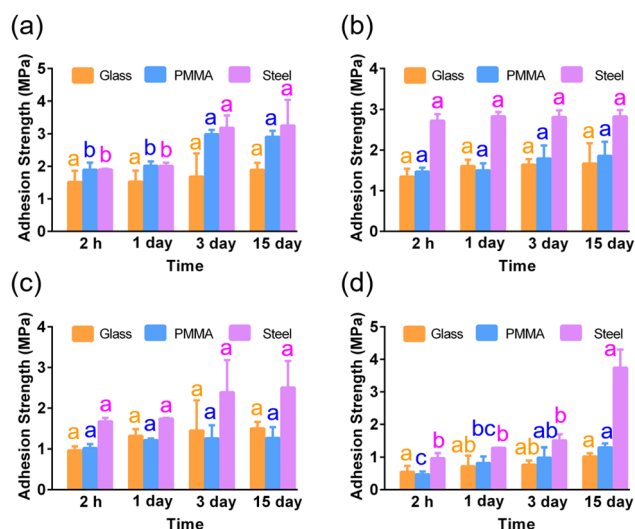


Fig. 3 Time-dependent adhesion strengths of poly[TA-MoS<sub>2</sub>] under water. (a) TA : MoS<sub>2</sub> = 1 : 1; (b) TA : MoS<sub>2</sub> = 5 : 1; (c) TA : MoS<sub>2</sub> = 10 : 1; (d) TA : MoS<sub>2</sub> = 100 : 1. Different letters signify significant differences at  $p < 0.05$ .

When poly[TA-MoS<sub>2</sub>] was exposed to laser light at 810 nm, its adhesion strength to glass decreased significantly (Fig. 4c). For instance, the adhesion strengths of poly[TA-MoS<sub>2</sub>]<sub>1/1</sub> at different laser irradiation times were 1.50 (0 min), 1.32 (0.5 min), 1.00 (1.0 min), and 0.56 MPa (2.0 min). The attenuation in the adhesion capacity of poly[TA-MoS<sub>2</sub>] exemplifies that MoS<sub>2</sub> can absorb laser light and transform it into heat energy, increasing the temperature of samples from 25 °C to 41 °C (Fig. 4a).

Based on the reversible temperature-dependent rheological and adhesion results, the potential of poly[TA-MoS<sub>2</sub>] as a high-performance 3D printing material was further investigated.

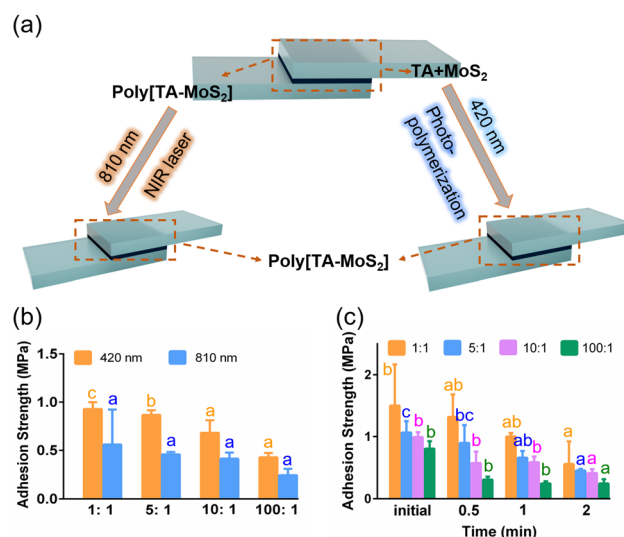
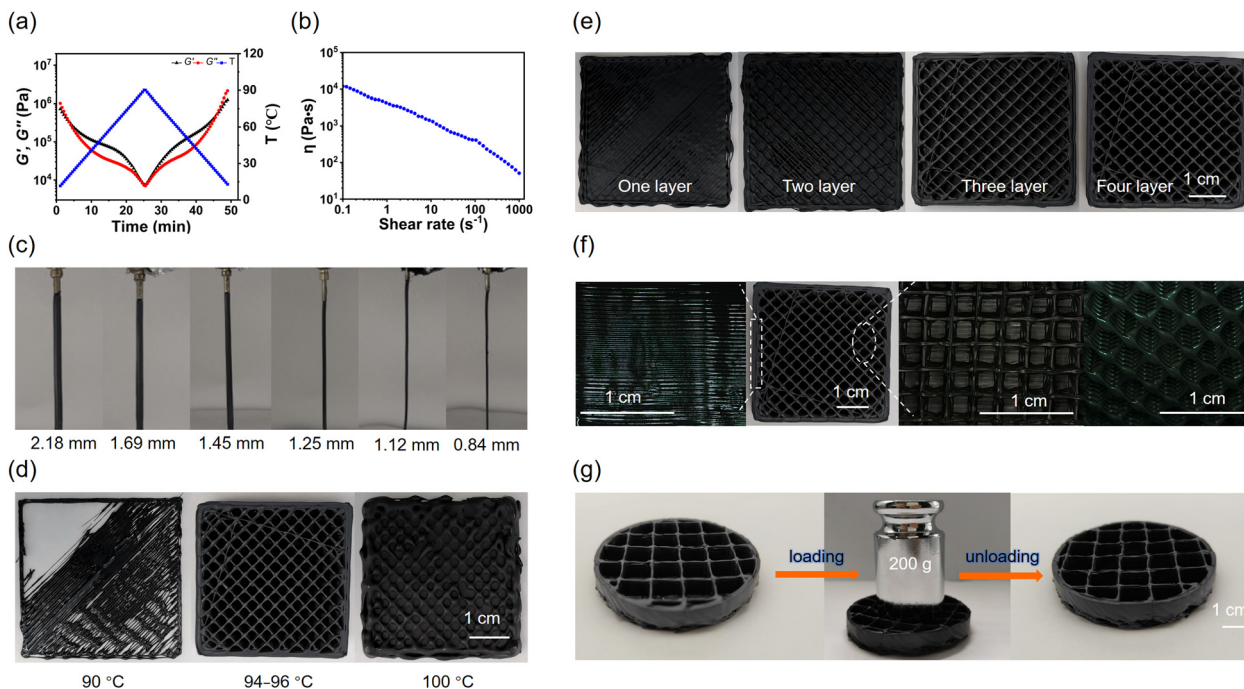


Fig. 4 The adhesion performance of poly[TA-MoS<sub>2</sub>]. (a) The schematic representation of the photo-sensitive adhesion behavior of poly[TA-MoS<sub>2</sub>]; (b) adhesion strengths of poly[TA-MoS<sub>2</sub>] irradiated with light (2 minutes, 420 nm, 810 nm laser, glass substrate); (c) time-dependent adhesion strengths of poly[TA-MoS<sub>2</sub>] (810 nm laser, glass substrate). Different letters signify significant differences at  $p < 0.05$ .

Rheological tests showed that poly[TA-MoS<sub>2</sub>] was thermally stable and had shear thinning behavior (Fig. 5a and b and Fig. S18, ESI<sup>†</sup>). Smooth filaments of poly[TA-MoS<sub>2</sub>] with different diameters were successfully obtained by thermal-processing technology, indicating that poly[TA-MoS<sub>2</sub>] is suitable for 3D FDM printing (Fig. 5c). A customized 3D printer was used to print 3D models using poly[TA-MoS<sub>2</sub>]. The printing temperature is one of the most important factors in the 3D printing process.<sup>41–44</sup> As shown in Fig. 5d, a low operating



**Fig. 5** Thermal processing of poly[TA-MoS<sub>2</sub>]. (a)  $G'$  and  $G''$  values of poly[TA-MoS<sub>2</sub>] in the reversible temperature-dependent rheological tests; (b) shear rate-dependent viscosity of poly[TA-MoS<sub>2</sub>] at 90 °C; (c) poly[TA-MoS<sub>2</sub>] filaments with different diameters; (d) 3D printing of poly[TA-MoS<sub>2</sub>] at different temperatures. (e) Bottom-up 3D printing process of poly[TA-MoS<sub>2</sub>]; (f) 3D-printed models of poly[TA-MoS<sub>2</sub>]. (g) Weight-loading test of poly[TA-MoS<sub>2</sub>]. Poly[TA-MoS<sub>2</sub>]<sub>10/1</sub> was used for 3D printing.

temperature led to failure in the extrusion of poly[TA-MoS<sub>2</sub>], while a very high temperature resulted in a long curing time. After multiple tests, the optimum temperature for 3D printing using poly[TA-MoS<sub>2</sub>] was determined to be between 94 °C and 96 °C. Intact and flexible models with high resolution were obtained *via* layer-by-layer printing of the molten poly[TA-MoS<sub>2</sub>] fibers (Fig. 5e). The printed poly[TA-MoS<sub>2</sub>] samples exhibited multiple layers (>20), smooth surface morphologies, and complicated structures. The poly[TA-MoS<sub>2</sub>] fibers could be easily identified from the printed structures. The printed poly[TA-MoS<sub>2</sub>] samples were self-standing and highly stable. For example, when a printed porous sample (diameter: 6 cm; height: 1.5 cm) was pressed using a 200 g weight for more than 48 h, no permanent deformation or fracture was observed in the printed structure. After storing under water or at ambient conditions for more than 90 days, there were no changes in the shape and structure of the printed poly[TA-MoS<sub>2</sub>], indicating its long-term stability in 3D printing (Fig. 5g and Fig. S19 and S20, ESI<sup>†</sup>).

In summary, an organic/inorganic hybrid supramolecular soft material was constructed by the dynamic covalent/non-covalent polymerization of two small monomers, TA and MoS<sub>2</sub>. Poly[TA-MoS<sub>2</sub>] exhibits strong and long-lasting adhesion performance on various hydrophilic surfaces, including glass, steel, and PMMA. Due to the photopolymerization and thermal depolymerization of TA, the adhesion strength and effect of poly[TA-MoS<sub>2</sub>] can be easily and effectively controlled by light irradiation at different wavelengths. Because of its thermal responsiveness, models of varied sizes and complicated structures can be obtained by 3D printing. This study not only

highlights the importance of inorganic compounds in the fabrication of TA materials, but also sheds light on the development of new 3D printing consumables.

## Author contributions

S. D. and S. L. supervised the project and designed the experiments. Y. Zhang, W. Yi and J. Pan performed all the experiments and characterization, analysed the data, and participated in the writing of the manuscript. All authors commented on the manuscript.

## Data availability

The data supporting this article have been included as part of ESI.<sup>†</sup>

## Conflicts of interest

The authors declare conflicts to declare.

## Acknowledgements

The authors gratefully acknowledge the National Natural Science Foundation of China (22271087), the Outstanding Youth Scientist Foundation of Hunan Province (2021JJ10010), the Huxiang Young Talent Program from Hunan Province (2018RS3036).

## References

- 1 Q. Zhang, C.-Y. Shi, D.-H. Qu, Y.-T. Long, B. L. Feringa and H. Tian, *Sci. Adv.*, 2018, **4**, eaat8192.
- 2 Y. Wang, S. Sun and P. Wu, *Adv. Funct. Mater.*, 2021, **31**, 2101494.
- 3 C. Cui, L. Mei, D. Wang, P. Jia, Q. Zhou and W. Liu, *Nat. Commun.*, 2023, **14**, 7707.
- 4 K. Endo, T. Shiroy, N. Murata, G. Kojima and T. Yamanaka, *Macromolecules*, 2004, **37**, 3143–3150.
- 5 B. Sieredzinska, Q. Zhang, K. J. van den Berg, J. Flapper and B. L. Feringa, *Chem. Commun.*, 2021, **57**, 9838–9841.
- 6 C. Chen, X. Yang, S.-J. Li, C. Zhang, Y.-N. Ma, Y.-X. Ma, P. Gao, S.-Z. Gao and X.-J. Huang, *Green Chem.*, 2021, **23**, 1794–1804.
- 7 Q. Zhang, Y.-X. Deng, H.-X. Luo, C.-Y. Shi, G. M. Geise, B. L. Feringa, H. Tian and D.-H. Qu, *J. Am. Chem. Soc.*, 2019, **141**, 12804–12814.
- 8 C.-Y. Shi, D.-D. He, B.-S. Wang, Q. Zhang, H. Tian and D.-H. Qu, *Angew. Chem., Int. Ed.*, 2023, **62**, e202214422.
- 9 Y. Liu, Y. Jia, Q. Wu and J. S. Moore, *J. Am. Chem. Soc.*, 2019, **141**, 17075–17080.
- 10 Q. Zhang, Y. Deng, C.-Y. Shi, B. L. Feringa, H. Tian and D.-H. Qu, *Matter*, 2021, **4**, 1352–1364.
- 11 K. Zhang, J. Zhang, Y. Liu, Z. Wang, C. Yan, C. Song, C. Gao and Y. Wu, *J. Colloid Interface Sci.*, 2021, **599**, 360–369.
- 12 W. Zheng, L. Xu, Y. Li, Y. Huang, B. Li, Z. Jiang and G. Gao, *J. Colloid Interface Sci.*, 2021, **594**, 584–592.
- 13 Y. Deng, Q. Zhang, C. Shi, R. Toyoda, D.-H. Qu, H. Tian and B. L. Feringa, *Sci. Adv.*, 2022, **8**, eabk3286.
- 14 C.-Y. Shi, D.-D. He, Q. Zhang, F. Tong, Z.-T. Shi, H. Tian and D.-H. Qu, *Natl. Sci. Rev.*, 2023, **10**, nwac139.
- 15 H. Qiao, B. Wu, S. Sun and P. Wu, *J. Am. Chem. Soc.*, 2024, **146**, 7533–7542.
- 16 C. Cui, F. Wang, X. Chen, T. Xu, Z. Li, K. Chen, Y. Guo, Y. Cheng, Z. Ge and Y. Zhang, *Adv. Funct. Mater.*, 2024, **34**, 2315469.
- 17 C. Cui, B. Liu, T. Wu, Y. Liu, C. Fan, Z. Xu, Y. Yao and W. Liu, *J. Mater. Chem. A*, 2022, **10**, 1257–1269.
- 18 J. Li, Y. Zhang, Q. Zhang, C. Cai, F. Li and S. Dong, *Adv. Mater. Interfaces*, 2023, **10**, 2202005.
- 19 J. Chen, D. Guo, S. Liang and Z. Liu, *Polym. Chem.*, 2020, **11**, 6670–6680.
- 20 H.-T. Zhang, L.-K. Hou, G.-W. Chu, J.-X. Wang, L.-L. Zhang and J.-F. Chen, *Chem. Eng. J.*, 2024, **482**, 148816.
- 21 X. Yang, B. Zhang, J. Li, M. Shen, H. Liu, X. Xu and S. Shang, *Carbohydr. Polym.*, 2023, **313**, 120813.
- 22 Q. Zhang, W. Wang, C. Cai, S. Wu, J. Li, F. Li and S. Dong, *Mater. Horiz.*, 2022, **9**, 1984–1991.
- 23 Z. Chen, C. Song, X. Lian, B. Xu and Y. Wang, *Adv. Funct. Mater.*, 2024, DOI: [10.1002/adfm.202400829](https://doi.org/10.1002/adfm.202400829).
- 24 K. Zhang, Z. Wang, J. Zhang, Y. Liu, C. Yan, T. Hu, C. Gao and Y. Wu, *Eur. Polym. J.*, 2021, **156**, 110618.
- 25 X. Chen, C. Hu, Y. Wang, T. Li, J. Jiang, J. Huang, S. Wang, W. Dong and J. Qiao, *Adv. Sci.*, 2024, **11**, 2304946.
- 26 J. Liu, X. Li, K. Chen, Y. Li, S. Feng, P. Su, Y. Zou, Y. Li and W. Wang, *Macromol. Rapid Commun.*, 2023, **44**, 2300282.
- 27 S. Luo, N. Wang, Y. Pan, B. Zheng, F. Li and S. Dong, *Small*, 2024, **20**, 2310839.
- 28 Y. Zhang, C. Cai, K. Xu, X. Yang, L. Yu, L. Gao and S. Dong, *Mater. Horiz.*, 2024, **11**, 1315–1324.
- 29 D. He, Z. Wang, X. Zeng, J. Fan, L. Ren, G. Du, R. Sun and X. Zeng, *ACS Appl. Mater. Interfaces*, 2022, **14**, 33912–33921.
- 30 W. Fang, Z. Mu, Y. He, K. Kong, K. Jiang, R. Tang and Z. Liu, *Nature*, 2023, **619**, 293–299.
- 31 Y. Liu, G. Wang, F. Luo, H. Li, M. Zhu, X. Liu, S. A. Yang and S. Liu, *Chem. Asian J.*, 2021, **16**, 1756–1761.
- 32 G. Yao, F. Li and S. Dong, *Chem. Eng. Sci.*, 2023, **281**, 119164.
- 33 J. Chen, T. Yuan and Z. Liu, *Biomater. Sci.*, 2020, **8**, 6235–6245.
- 34 K.-X. Hou, S.-P. Zhao, D.-P. Wang, P.-C. Zhao, C.-H. Li and J.-L. Zuo, *Adv. Funct. Mater.*, 2021, **31**, 2107006.
- 35 X. Peng, Y. Li, T. Li, Y. Li, Y. Deng, X. Xie, Y. Wang, G. Li and L. Bian, *Adv. Sci.*, 2022, **9**, 2203890.
- 36 C.-Y. Shi, Q. Zhang, B.-S. Wang, M. Chen and D.-H. Qu, *ACS Appl. Mater. Interfaces*, 2021, **13**, 44860–44867.
- 37 H. Guo, W. Zhang, Z. Jia, P. Wang, Q. Shao, H. Shen, J. Li, Q. Chen and B. Chi, *Adv. Funct. Mater.*, 2024, DOI: [10.1002/adfm.202401529](https://doi.org/10.1002/adfm.202401529).
- 38 H. Huang, H. Wang, L. Sun, R. Zhang, L. Zhang, Z. Wu, Y. Zheng, Y. Wang, W. Fu, Y. Zhang, R. E. Neisiany and Z. You, *CCS Chem.*, 2024, **6**, 761–773.
- 39 J. Zhang, Z. Chen, Y. Zhang, S. Dong, Y. Chen and S. Zhang, *Adv. Mater.*, 2021, **33**, 2100962.
- 40 H. K. Moon, S. H. Lee and H. C. Choi, *ACS Nano*, 2009, **3**, 3707–3713.
- 41 Y. Zhang, C. Cai, F. Li and S. Dong, *Small*, 2023, **19**, 2300857.
- 42 C. Cai, S. Wu, Y. Zhang, F. Li, Z. Tan and S. Dong, *Adv. Sci.*, 2022, **9**, 2203630.
- 43 K. Cao, M. Wu, J. Bai, Z. Wen, J. Zhang, T. Wang, M. Peng, T. Liu, Z. Jia, Z. Liang and L. Jiang, *Adv. Funct. Mater.*, 2022, **32**, 2202360.
- 44 J. Chen, X. Liu, Y. Tian, W. Zhu, C. Yan, Y. Shi, L. B. Kong, H. J. Qi and K. Zhou, *Adv. Mater.*, 2022, **34**, 2102877.